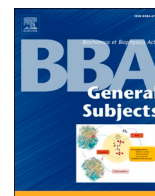


Contents lists available at [ScienceDirect](https://www.sciencedirect.com)

BBA - General Subjects

journal homepage: www.elsevier.com/locate/bbagen

Novel inhibitors of human glucose-6-phosphate dehydrogenase (HsG6PD) affect the activity and stability of the protein

Edson Jiovany Ramírez-Nava^{a,b,1}, Beatriz Hernández-Ochoa^{c,d,1}, Gabriel Navarrete-Vázquez^e, Roberto Arreguín-Espinosa^f, Daniel Ortega-Cuellar^g, Abigail González-Valdez^h, Víctor Martínez-Rosas^{a,d}, Laura Morales-Luna^{a,b}, Josué Martínez-Miranda^e, Edgar Sierra-Palaciosⁱ, Luz María Rocha-Ramírez^j, Lucia De Franceschi^k, Jaime Marcial-Quino^{l,*}, Saúl Gómez-Manzo^{a,*}

^a Laboratorio de Bioquímica Genética, Instituto Nacional de Pediatría, Secretaría de Salud, Ciudad de México 04530, Mexico

^b Posgrado en Ciencias Biológicas, Universidad Nacional Autónoma de México, 04510 Ciudad de México, Mexico

^c Laboratorio de Inmunoquímica, Hospital Infantil de México Federico Gómez, Secretaría de Salud, Ciudad de México 06720, Mexico

^d Programa de Posgrado en Biomedicina y Biotecnología Molecular, Escuela Nacional de Ciencias Biológicas, Instituto Politécnico Nacional, Ciudad de México 11340, Mexico

^e Facultad de Farmacia, Universidad Autónoma del Estado de Morelos, Av. Universidad 1001, Chamilpa, Cuernavaca, Morelos 62209, Mexico

^f Departamento de Química de Biomacromoléculas, Instituto de Química, Universidad Nacional Autónoma de México, Ciudad de México 04510, Mexico

^g Laboratorio de Nutrición Experimental, Instituto Nacional de Pediatría, 04530 Secretaría de Salud, Mexico

^h Departamento de Biología Molecular y Biotecnología, Instituto de Investigaciones Biomédicas, Universidad Nacional Autónoma de México, Ciudad de México 04510, Mexico

ⁱ Colegio de Ciencias y Humanidades, Plantel Casa Libertad, Universidad Autónoma de la Ciudad de México, Ciudad de México 09620, Mexico

^j Unidad de Investigación en Enfermedades Infecciosas, Hospital Infantil de México Federico Gómez, Secretaría de Salud Dr. Márquez No. 162, Col Doctores, Delegación Cuauhtémoc, Ciudad de México 06720, Mexico

^k Department of Medicine, University of Verona and AOUI Verona, Policlinico GB Rossi, Verona, Italy

^l Consejo Nacional de Ciencia y Tecnología (CONACYT), Instituto Nacional de Pediatría, Secretaría de Salud, Ciudad de México 04530, Mexico

ARTICLE INFO

Keywords:

HsG6PD inhibition
Second-order inactivation constant
Inhibition type
Structural perturbation
Molecular docking

ABSTRACT

Background: The pentose phosphate pathway (PPP) has received significant attention because of the role of NADPH and R-5-P in the maintenance of cancer cells, which are necessary for the synthesis of fatty acids and contribute to uncontrollable proliferation. The HsG6PD enzyme is the rate-limiting step in the oxidative branch of the PPP, leading to an increase in the expression levels in tumor cells; therefore, the protein has been proposed as a target for the development of new molecules for use in cancer.

Methods: Through in vitro studies, we assayed the effects of 55 chemical compounds against recombinant HsG6PD. Here, we present the kinetic characterization of four new HsG6PD inhibitors as well as their functional and structural effects on the protein. Furthermore, molecular docking was performed to determine the interaction of the best hits with HsG6PD.

Results: Four compounds, JMM-2, CCM-4, CNZ-3, and CNZ-7, were capable of reducing HsG6PD activity and showed noncompetitive and uncompetitive inhibition. Moreover, experiments using circular dichroism and fluorescence spectroscopy showed that the molecules affect the structure (secondary and tertiary) of the protein as well as its thermal stability. Computational docking analysis revealed that the interaction of the compounds with the protein does not occur at the active site.

Conclusions: We identified two new compounds (CNZ-3 and JMM-2) capable of inhibiting HsG6PD that, compared to other previously known HsG6PD inhibitors, showed different mechanisms of inhibition.

General significance: Screening of new inhibitors for HsG6PD with a future pharmacological approach for the study and treatment of cancer.

* Corresponding authors.

E-mail addresses: jmarcialq@ciencias.unam.mx (J. Marcial-Quino), saulmanzo@ciencias.unam.mx (S. Gómez-Manzo).

¹ These authors contributed equally to this work.

<https://doi.org/10.1016/j.bbagen.2020.129828>

Received 31 August 2020; Received in revised form 26 November 2020; Accepted 14 December 2020

Available online 23 December 2020

0304-4165/© 2020 Elsevier B.V. All rights reserved.

1. Introduction

The pentose phosphate pathway (PPP) is the metabolic pathway known as the hexose monophosphate shunt and consumes glucose-6-phosphate as a primary substrate. The PPP is a metabolic pathway from which a cell that is proliferating is supplied with both the nucleotide precursors needed for proliferation and reduced nicotinamide adenine dinucleotide phosphate (NADPH), a fundamental molecule for the synthesis of fatty acids, which are essential in the synthesis of cell membranes [1]. Additionally, NADPH is used for intracellular ROS detoxification because the electrons of NADPH are used by the glutathione reductase enzyme for the generation of reduced glutathione (GSH), providing the first line of defense against ROS and preventing the accumulation of these toxic species in the cell [2–5].

The G6PD enzyme catalyzes the first and rate-limiting step of the oxidative phase in the pentose phosphate pathway (PPP), and together with the 6-phosphogluconate dehydrogenase (6PGD) enzyme, it produces the reduced form of nicotinamide adenine dinucleotide phosphate (NADPH) [6]. Recently, it has been observed that in diseases such as diabetes, heart failure, pulmonary insufficiency, and cancer, human G6PD (HsG6PD) activity is deregulated [7–11]. Furthermore, several researchers have paid considerable attention to the PPP, especially in the role of HsG6PD in cancer. In this sense, various studies have reported that there is an increase in the levels of expression in the mRNA of the *G6PD* gene in several types of neoplasms, such as breast [12], colon cancer [13], and gliomas [14]. The latter is due to the crucial role of NADPH and ribose-5-phosphate in maintaining cancer cells, which are required for the synthesis of fatty acids, contributing to uncontrollable proliferation and increased cell survival under stress conditions. Moreover, it has been shown that the PPP plays a role in cisplatin resistance. Cisplatin is the first-line treatment for different types of solid tumors, and the overexpression of this gene combined with high activity of G6PD increases drug resistance [15]. In addition, the increase in glucose in the PPP to support anabolic demands in cancer increases oxidative stress, endoplasmic reticulum stress, and apoptosis [16].

HsG6PD is the rate-limiting step in the oxidative branch of the PPP [1], and this enzyme is highly regulated in normal cells. Transcriptional regulation of the *G6PD* gene is carried out by the interaction of mechanistic target of rapamycin complex 1 (mTORC1) with the transcriptional factors sterol regulatory element-binding proteins (SREBP) and Tap73 in the *G6PD* gene [17,18] and by posttranscriptional signaling cascades such as the 1-phosphatidylinositol 3-kinase-protein kinase B pathway (PI3K-AKT) through p53 [19], phosphatidylinositol-3,4,5-triphosphate 3-phosphatase (PTEN) [20] and ataxia-telangiectasia mutated kinase (ATM) through HSP1 [21] as well as alterations in the NADPH/NADP⁺ ratio [22]. However, in tumor cells, the regulation of HsG6PD is altered by genetic and metabolic modifications. Compared to normal cells, higher expression of HsG6PD and greater activity have been reported [12]; the inhibition of IRE1 (inositol requiring enzyme 1) in U87 glioblastoma cells modifies the hypoxia response and increases the gene expression of some enzymes of the PPP, including G6PD [23]. It has been observed that this overexpression of HsG6PD in cancer cells confers proliferative advantages and greater protection against oxidative damage [6,24], leading to increased resistance by tumor cells to chemotherapy treatments such as the use of cisplatin [12]. Based on the above, different therapeutic alternatives have been studied to try to affect the metabolism of tumor cells. One option has been to inhibit the activity of HsG6PD to attempt to reduce the uncontrollable proliferation presented by cancer cells as well as to make them vulnerable to traditional therapies. Previously, chemical compounds that reduce G6PD activity, such as dehydroepiandrosterone (DHEA) and 6-aminonicotinamide (6AN), have been analyzed; however, these inhibitors have not been used for therapy because they have severe side effects, such as nerve damage and vitamin B deficiency [25]. On the other hand, Preuss et al. [26] proposed novel G6PD inhibitors for recombinant human G6PD and found that only one inhibitor had a negative effect on cellular

viability in the MCF10 model of mammary carcinoma. Naringenin (a flavanone) has also been proposed as an inhibitor of glial cell tumorigenesis in glioma C6 cells implanted in rats, modifying metabolic markers, including G6PD enzyme activity [27]; the antioxidant and antiproliferative effects of curcumin and polyunsaturated fatty acids have also been shown in rat glioma C6 cells [28,29]. Currently, *G6PD* gene expression is proposed as a biomarker for the risk and prognosis of and chemosensitivity to- glioma [30].

Based on the necessity of finding new inhibitors against HsG6PD, in this study, we investigated the effects of an in-house library comprising 55 synthetic compounds on the activity of the human recombinant G6PD enzyme. Furthermore, we found and described HsG6PD inhibition by four of these compounds, where **JMM-2**, **CCM-4**, **CNZ-3**, and **CNZ-7** compounds were also capable of reducing HsG6PD activity and showed noncompetitive and uncompetitive inhibition. It is interesting to note that this is the first time that the effect of these compounds on the secondary and tertiary structure of the protein has been observed as well as thermal stability (global stability of the protein) in the HsG6PD protein. Finally, by molecular blind docking, we determined the possible structural inhibitor binding site in this enzyme.

2. Materials and methods

2.1. Expression and purification of recombinant HsG6PD protein

All the assays in the present study were performed using recombinant human glucose-6-phosphate dehydrogenase (HsG6PD). The protein was overexpressed and purified according to the reported method by Gómez-Manzo et al. [3]. The protein purity was verified with 12% sodium dodecyl sulfate-polyacrylamide gel electrophoresis (SDS-PAGE), and then the gel was stained with colloidal Coomassie (R-250) (Sigma-Aldrich, San Luis, Misuri, USA).

2.2. Compounds library and high-screening assay

The high screening assay was performed using 55 compounds belonging to an in-house library synthesized in the Medicinal Chemistry Laboratory from Universidad Autónoma from Estado de Morelos, Faculty of Pharmacy (Supplementary Materials Table S1). In-house libraries are advantageous in discovering novel bioactive small molecules. All assays were performed with 0.2 mg/mL HsG6PD protein, and the compounds were tested to a final concentration of 400 μ M. Dimethyl sulfoxide (DMSO) was used to solubilize the compounds, and we verified that the final concentration of DMSO did not exceed 5% and did not affect the catalytic activity of HsG6PD [26]. The enzyme was incubated with each of the compounds for two hours at 37 °C, and then the residual activity of HsG6PD was measured with a standard reaction mixture (100 mM Tris-HCl buffer, pH 8.0, 3 mM MgCl₂, 200 μ M G6P (~5-fold of the K_m value = 38.4 μ M), and 35 μ M NADP⁺ (~5-fold of the K_m value = 35 μ M)), following NADPH production at 340 nm. The enzyme activity without compounds was adjusted to 100%. Compounds that inhibited HsG6PD activity by more than 50% were considered hit candidates to perform the following experiments. Three experiments were performed for this assay.

2.3. Orthogonal assays

Selected hit compounds (four compounds) were used to determine the IC₅₀ values (the concentration of the compound at which the protein loses 50% of its activity). The orthogonal assays were performed with 0.2 mg/mL HsG6PD protein previously incubated for 2 h at 37 °C with increasing concentrations ranging from 0 to 800 μ M of the four compounds selected in the high-screening experiment. Then, the residual HsG6PD activity was measured, and the initial velocities obtained were plotted versus compound concentration. The enzyme activity without compounds was adjusted to 100%. The IC₅₀ values were calculated using

the Origin 8.0® program. Three experiments were performed for this assay.

2.4. Second-order inactivation constant (k_2) of HsG6PD exposed to selected hit compounds

The second-order inactivation constant k_2 ($M^{-1} s^{-1}$) was used to determine the inactivation rate of each compound and to represent the rate of formation of the enzyme-inhibitor complex. First, the pseudo-first order inactivation rate constants (k_1) were obtained from 0 to 1 mM for the four compounds. The HsG6PD protein (0.2 mg/mL) was incubated with four fixed concentrations of each of the compounds, and at the indicated times, aliquots were withdrawn to determine residual activity. The residual activity data were fitted using the following mono-exponential decay equation $A_R = A_0 e^{-k_1 t}$ to obtain the pseudo-first order rate constant (k_1) values at each fixed concentration of compounds. Then, to obtain the second-order rate constants of inactivation, the k_1 values of each compound were plotted against the employed concentrations of each compound, and the second-order rate constant value of inactivation k_2 ($M^{-1} s^{-1}$) was obtained from the slope of these plots as previously described [31,32].

2.5. Determination of inhibition type

To determine the inhibition mechanism of the four selected hit compounds, we evaluated changes in the V_{max} and K_m parameters for the HsG6PD enzyme in the presence of four fixed concentrations of each of the compounds. The main kinetic parameters (K_m and V_{max}) were determined by measuring the initial rates at different substrate concentrations. Initial velocities for the G6P substrate were obtained by varying the G6P substrate (0 to 250 μM), while $NADP^+$ was fixed at a saturating concentration (~5-fold of the K_m value = 35 μM). For initial velocities of the $NADP^+$ substrate, this varied from 0 to 250 μM , and the G6P substrate was fixed at a saturating concentration (~5-fold of the K_m value = 38.4 μM). The parameters K_m and V_{max} for the four compounds were obtained by fitting the data to the Michaelis-Menten equation by nonlinear regression calculations using the Origin 8.0® program [3]. All the initial rate measurements were carried out in triplicate. The initial activities were fitted to the Michaelis-Menten equation by nonlinear regression calculations to obtain the parameters V_{max} and K_m . To determine the inhibition mechanism of the four compounds in the HsG6PD enzyme, the experimental data were analyzed using the double reciprocal plot method. The inactivation constant (K_i) was obtained by plotting the value of the slope obtained at each of the fixed concentrations of each compound in the double reciprocal graph against the concentration of the compound. Then, the data were adjusted to a linear regression model, where the interception with axis y was the determined K_i value (μM).

2.6. Structural studies of HsG6PD enzyme with the compounds

2.6.1. Circular dichroism (CD) and thermal stability assays

To determine whether the loss of HsG6PD activity caused by the inhibitors was due to alterations in the secondary structure of the protein, we performed a circular dichroism (CD) assay in the presence of each inhibitor. The secondary structure of the HsG6PD protein was analyzed by CD in a spectropolarimeter (Jasco J-810®, Inc., MD, USA). The protein was adjusted to 0.2 mg/mL with buffer P (50 mM phosphate pH 7.35), incubated for 2 h at 37 °C in the absence and presence of the compounds (IC_{50} of each compound) and loaded in a rectangular quartz cuvette with a 1 cm optical path. Spectra were recorded at 25 °C in ultraviolet circular dichroism (UV-CD) ranging from 200 to 260 nm by monitoring changes in the emission of the molar ellipticity of the spectra at 222 and 208 for the α -helices and β -sheets, respectively. Spectra of the blanks (buffer P solution containing each of the compounds) were subtracted from all the obtained spectra that contained the protein [33].

The curves were plotted using the Origin 8.0® program.

Furthermore, the thermal denaturation of HsG6PD in the presence of the four inhibitors was performed by monitoring the unfolded fraction at 222 nm as a function of temperature, ranging from 35 to 70 °C and increasing at a rate of 1 °C/2.5 min. The assay was performed in a spectropolarimeter Jasco J-8190, as previously reported [5]. The protein was adjusted to 0.2 mg/mL with buffer P and incubated for 2 h at 37 °C in the absence and presence of four compounds (IC_{50} of each compound). The data were adjusted with the Boltzmann equation using the Origin 8.0® program to obtain the T_m value (the temperature at which 50% of the protein is folded and 50% is unfolded, expressed as the melting temperature). Both experiments were performed in triplicate.

2.6.2. Intrinsic and extrinsic fluorescence assays

To evaluate the structural changes in HsG6PD with the four compounds, we performed intrinsic and extrinsic fluorescence assays. For the intrinsic fluorescence assay, the HsG6PD protein was adjusted to 0.1 mg/mL in buffer P and incubated for 2 h at 37 °C in the absence or presence of each of the compounds at the IC_{50} concentration. The intrinsic fluorescence spectra were recorded at 310–500 nm in a Perkin-Elmer LS-55 fluorescence spectrometer (Perkin Elmer®, Wellesley, MA, USA) using an excitation wavelength of 295 nm and slits of excitation and emission of 10 and 10 nm, respectively. The final spectrum was the average of five scans; later, each spectrum was subtracted from the spectra of the blank (buffer P solution containing each of the compounds without protein) [34].

Furthermore, we determined the extrinsic fluorescence of the HsG6PD enzyme in the presence of the four compounds by an 8-anilino-naphthalene-1-sulfonic acid (ANS) assay to monitor changes in the hydrophobic regions of the protein. The protein was incubated under the same conditions as the intrinsic fluorescence assay. Then, we recorded the fluorescence spectra from 400 to 600 nm in the presence of 25 mM ANS dissolved in methanol. The assay was carried out at 25 °C with a scanning rate of 200 nm/min. The samples were excited to 395 nm using slits of excitation and emission of 10 nm. The final spectrum was the average of five scans. Later, each spectrum was subtracted from the spectra of the blank (buffer P solution containing each of the compounds plus ANS).

2.7. Blind molecular docking

The crystal structure of HsG6PD [35] was downloaded from the Protein Data Bank (PDB ID: 2BHL, <http://www.rcsb.org/pdb>). The 3D structures of the compounds were generated in Chem-Draw Professional 16.0; they were assembled with Molecular Operating Environment (MOE) software. This crystal structure was complexed with two molecules of $NADP^+$ (structural and catalytic binding sites), which were maintained for the docking analysis, and the rest of the pockets were emptied, removing all the water molecules and heteroatoms from the PDB file; this process was performed using the open-source program PyMOL (The PyMOL Molecular Graphics System, Version 2.0 Schrödinger, LLC, New York, NY, USA). After this process, the protein was analyzed with the program Molecular Operating Environment (MOE) to verify that there were no incomplete domains or fragments, and system energy minimization was also performed.

2.7.1. Preparation of the ligand PDB files

The 3D structures of the docked compounds were obtained from MOE, reducing the system energy, and a protonated state was considered if the compounds had an ionic group. The files were saved as *.PDB files.

2.7.2. Preparation of the Pdbqt files

The *.pdbqt files of the receptor and the ligands were obtained using the Autodock Vina input in PyMOL, and because this was a “blind docking”, there was no need to define the binding pocket of the receptor.

2.7.3. Defining the grid box

The grid box parameters were defined using the AutoDock Vina input in PyMOL. In this case, no specific area was defined, so the entire protein was enclosed in the grid box, adding 5 Å in each axis to ensure that the entire protein was enclosed in the grid box. The total dimensions of the grid box were as follows: X: 72 Å, Y: 67 Å, and Z: 96 Å.

2.7.4. Docking

The docking was performed in Linux, performing 100 independent experiments and obtaining 10 results in each experiment, with a total of 1000 results per ligand. The affinity energies and the tridimensional configuration of each ligand were analyzed to select the best 100 results (both energy and tridimensional configurations were selected and categorized as reliable and repeatable results). For the affinity energies and tridimensional configuration, the mean and the standard deviation were calculated.

The docking protocols were validated by the redocking of NADP⁺ located in the HsG6PD catalytic binding site of 2BHL. A root-mean-square deviation (RMSD) value less than 2.0 Å between the cocystal coenzyme and the docked NADP⁺ was considered the parameter to determine that the docking calculations reproduced the conformation and orientation in the X-ray crystal of HsG6PD. Finally, the generated docking results were directly loaded into PyMOL (The PyMOL Molecular Graphics System, Version 2.0 Schrödinger, LLC, New York, NY, USA).

3. Results

3.1. Biochemical assays

3.1.1. Selection of HsG6PD inhibitors

High-throughput screening (HTS) assays were performed to identify molecules that modified the activity of the HsG6PD protein. Previously, Preuss et al. [26] found five compounds that are capable of inhibiting the activity of HsG6PD. Based on this information, we analyzed a library of 55 compounds with similar structures to those previously reported [26] at a final concentration of 400 μM, which were chemically similar to those reported by Preuss et al. [26], and we found that four chemical compounds, named **JMM-2**, **CCM-4**, **CNZ-3**, and **CNZ-7**, were also capable of reducing the activity of the human G6PD enzyme by more

than 40% (Table 1).

The compounds **JMM-2** and **CCM-4** are structurally similar, as both have a biphenyl ring in their structure; however, **JMM-2** comes from 3-phenylpropanoic acid and **CCM-4** from phenylacetic acid. We observed that of these two compounds, **JMM-2** showed the highest percentage of inhibition on recombinant HsG6PD with 89.5% inhibition (Table 1), while compound **CCM-4** derived from phenylacetic acid showed 47.3% inhibition of HsG6PD activity. These results could indicate that it is necessary for the molecule to have a carboxylic acid chain of at least three carbon atoms to achieve a percentage of enzyme inhibition greater than 80%; this feature is present in compound **JMM-2**.

On the other hand, compounds **CNZ-3** and **CNZ-7** are analogs of nitazoxanide, a well-known antiparasitic compound. Structurally, they have a 5-nitro-2-aminothiazole ring connected by a urea bridge with a benzamide ring. However, compound **CNZ-3** has a *p*-chloro substituent in the benzamide ring and showed 92.6% inhibition of HsG6PD activity, while compound **CNZ-7** has an *n*-butyl ether substituent in the same position—this radical has more volume and is less electronegative than the *p*-chloro substituent—and showed inhibition of 68.0% of HsG6PD activity (Table 1).

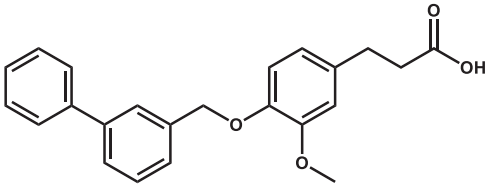
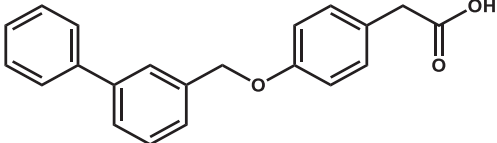
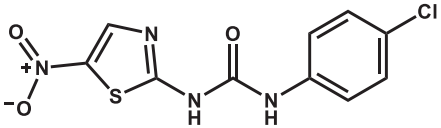
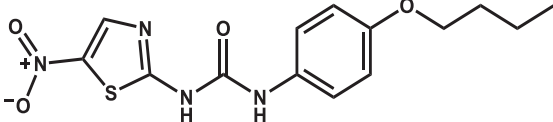
These results indicate that the inhibition of the HsG6PD enzyme depends on the structural characteristics and physicochemical properties of each compound. Furthermore, we observed that the inhibition was lower in the compounds that have more volume in their functional groups, as in the case of **CNZ-7**. The four chemical compounds selected in this first assay were used to perform biochemical and physicochemical assays (Table 1).

3.1.2. Orthogonal assay

Given that four compounds (**JMM-2**, **CCM-4**, **CNZ-3**, and **CNZ-7**) showed a high percentage of inhibition of HsG6PD, we analyzed the concentration response to determine the IC₅₀. The IC₅₀ values determined for the chemical compounds **JMM-2**, **CCM-4**, **CNZ-3**, and **CNZ-7** were 307 μM, 412 μM, 121 μM, and 274 μM, respectively. As seen in Fig. 1, compared to the other three compounds, the HsG6PD enzyme lost activity faster with the compound **CNZ-3**, showing a greater negative effect on the catalytic activity of HsG6PD at low concentrations. The differences in the IC₅₀ values between these chemical compounds were probably due to the structural differences that each compound presents,

Table 1

Synthetic compounds from an in-house library that showed an inhibition percentage greater than 40% on HsG6PD activity at a final concentration of 400 μM.

Chemical compounds	Structure	Inhibition (%) at [400 μM]
JMM-2		89.5
CCM-4		47.3
CNZ-3		92.6
CNZ-7		68.0

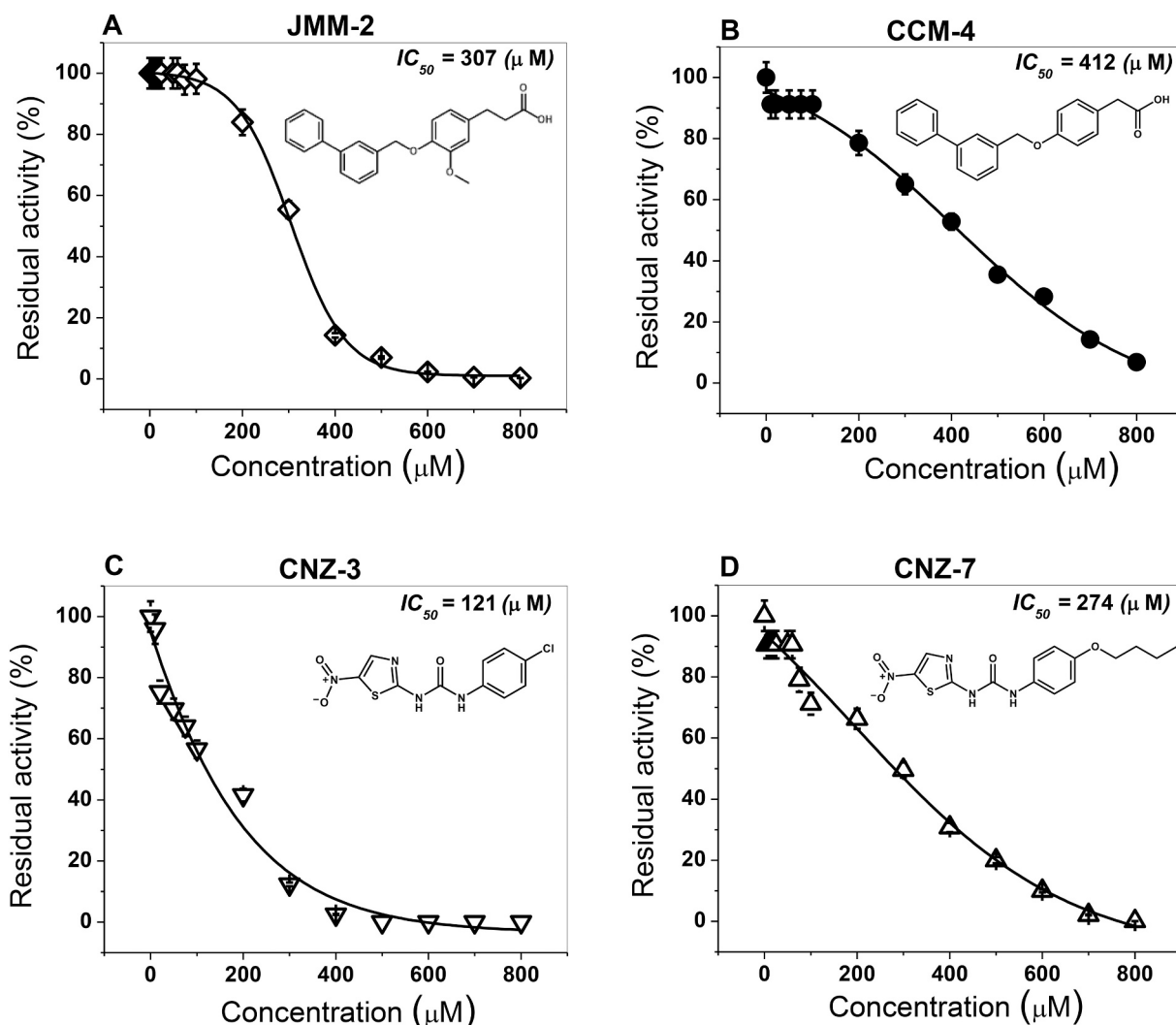


Fig. 1. Inactivation of HsG6PD with the compounds **JMM-2**, **CCM-4**, **CNZ-3**, and **CNZ-7**. The protein concentration of HsG6PD was adjusted to 0.2 mg/mL and incubated with increasing concentrations of each of the compounds (0–800 μM) for 2 h at 37 $^{\circ}\text{C}$. The IC_{50} values for each compound were determined by plotting the relative activity of HsG6PD versus compound concentrations (panel A–D). All assays for each compound were performed in triplicate. The bars represent the standard error.

as was observed in the high-throughput screening (HTS) assay. It is interesting to note that the four compounds tested here inhibited the activity of HsG6PD to different extents, and the inhibitory effect revealed a concentration-dependent inhibition (Fig. 1).

3.1.3. Second-order inactivation constants (k_2) of HsG6PD in the presence of four compounds

To determine the ratio formation of the complex enzyme inhibitors of each of the chemical compounds with the HsG6PD enzyme, we first calculated the pseudo-first order inactivation constants (k_1) after the enzyme was incubated with different fixed concentrations of each compound, and the initial velocities were measured at different incubation times. The synthetic compounds, **JMM-2** and **CCM-4**, showed single-exponential decays of time-course inactivation and had a negative effect on the catalytic activity of the HsG6PD enzyme (Fig. 2A, C). From this plot, we calculated the k_1 values for each compound and plotted them against the concentrations (Fig. 2B, D, respectively), and linear behavior was obtained. The calculated k_2 value for **JMM-2** was $0.50 \text{ M}^{-1} \text{ s}^{-1}$, while for **CCM-4**, the calculated k_2 value was $0.63 \text{ M}^{-1} \text{ s}^{-1}$.

On the other hand, the **CNZ-3** and **CNZ-7** compounds also showed single-exponential decays of time-course inactivation (from 0 to 120 min) (Fig. 2E, G). As seen in Fig. 2, as the concentration of the chemical

compounds **CNZ-3** and **CNZ-7** increased, the HsG6PD enzyme lost catalytic activity in a shorter incubation time; as expected, in the HsG6PD enzyme that was not incubated with the chemical compounds, the enzymatic activity remained intact. The calculated k_1 values were plotted against the concentrations of each of the compounds (Fig. 2F, H). The calculated k_2 value for **CNZ-3** was $0.66 \text{ M}^{-1} \text{ s}^{-1}$, while the k_2 value calculated for **CNZ-7** was $0.83 \text{ M}^{-1} \text{ s}^{-1}$. This indicated that the compound **CNZ-7**, which has a higher k_2 value, inactivates the enzyme HsG6PD faster than **CNZ-3**. This difference in the reactivity between these pairs of compounds is because they present different radicals, i.e., *p*-chloro for **CNZ-3**, while compound **CNZ-7** has an *n*-butyl-ether substituent in the same position.

According to the k_2 values obtained for the four chemical compounds, **JMM-2** and **CCM-4** compounds are slower to form the enzyme-inhibitor complex than the **CNZ-7** and **CNZ-3** compounds, which showed higher k_2 values. For all compounds, we observed that the inhibition was concentration-dependent, which indicates that the four chemical compounds showed direct inhibition of HsG6PD activity. Finally, it is interesting to note that this is the first time that k_2 values have been reported for G6PD inhibitors.

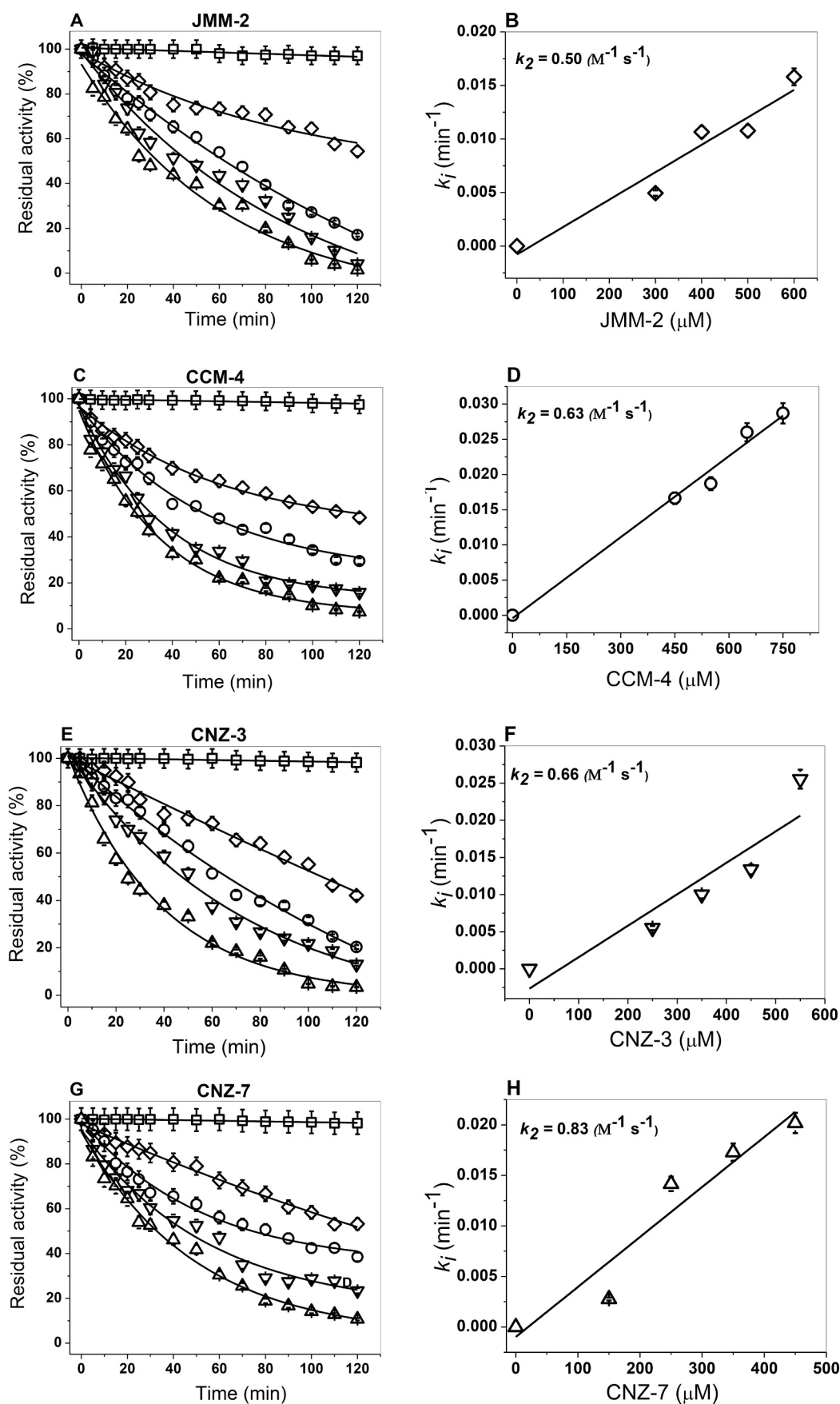


Fig. 2. Inactivation assay with JMM-2, CCM-4, CNZ-3, and CNZ-7 chemical compounds. The HsG6PD enzyme was adjusted to 0.2 mg/mL and incubated at 37 °C with different concentrations of (A) JMM-2 ($\square = 0 \mu\text{M}$, $\diamond = 300 \mu\text{M}$, $\circ = 400 \mu\text{M}$, $\nabla = 500 \mu\text{M}$, and $\Delta = 600 \mu\text{M}$). (C) CCM-4 ($\square = 0 \mu\text{M}$, $\diamond = 450 \mu\text{M}$, $\circ = 550 \mu\text{M}$, $\nabla = 650 \mu\text{M}$, and $\Delta = 750 \mu\text{M}$). (E) CNZ-3 ($\square = 0 \mu\text{M}$, $\diamond = 250 \mu\text{M}$, $\circ = 350 \mu\text{M}$, $\nabla = 450 \mu\text{M}$, and $\Delta = 550 \mu\text{M}$). (D) CNZ-7 ($\square = 0 \mu\text{M}$, $\diamond = 150 \mu\text{M}$, $\circ = 250 \mu\text{M}$, $\nabla = 350 \mu\text{M}$, and $\Delta = 450 \mu\text{M}$). To determine the pseudo-first order rate constant values (k_i) for each compound, the initial velocity data were fitted using the mono-exponential decay equation: $A_R = A_0 e^{-k_i t}$. The second-order rate constant values of inactivation (k_2) of each of the compounds (B) JMM-2, (D) CCM-4, (F) CNZ-3, and (H) CNZ-7 were obtained by fitting the calculated k_i value versus the concentration of the corresponding compound and adjusting to a linear regression model. All experiments were performed in triplicate. The bars represent the standard error.

3.1.4. Determination of inhibition type

To determine the mechanism of action of the four synthetic compounds on the activity of HsG6PD, we created Michaelis–Menten curves in the presence of physiological substrates G6P and NADP⁺ and in the presence of increasing inhibitor concentrations (Supplementary Fig. S1). The initial activities were fitted to the Michaelis–Menten equation by nonlinear regression calculations to obtain the parameters V_{\max} and K_m . As seen in Supplementary Fig. S1, when the enzyme HsG6PD was incubated with different concentrations of the four inhibitors, the specific activity (I. U) for both substrates was significantly decreased.

From the Michaelis–Menten plots of HsG6PD in the presence of increased inhibitor concentrations, we determined the type of inhibition. As seen in Supplementary Fig. S2, compound **JMM-2** showed noncompetitive-type inhibition of G6P and NADP⁺ substrates because the V_{\max} values for both substrates decreased (Supplementary Fig. S2A–B), while the K_m value remained unchanged even at different inhibitor concentrations. Compound **CCM-4** showed uncompetitive-type inhibition for both physiological substrates because the K_m and V_{\max} values decreased as the inhibitor concentrations increased (Supplementary Fig. S2C–D). It is important to note that the four compounds evaluated in this work showed noncompetitive and uncompetitive inhibition and that none of them are competitive-type inhibitors.

CNZ-3 showed noncompetitive-type inhibition of the G6P substrate because the V_{\max} decreased in the presence of the inhibitor, but the K_m was not influenced as the inhibitor concentration increased (Supplementary Fig. S2E). However, for the NADP⁺ substrate, the inhibition

was of the uncompetitive type because the V_{\max} and K_m decreased with all inhibitor concentrations (Supplementary Fig. S2F). Finally, with respect to the **CNZ-7** inhibitor, we determined uncompetitive-type inhibition for both physiological substrates (G6P and NADP⁺) because the values of V_{\max} and K_m decreased in the presence of the four fixed concentrations of the inhibitor (Supplementary Fig. S2G–H).

To determine which of the inhibitors have a greater HsG6PD enzyme binding affinity, we calculated the inactivation constants (K_i) for the four inhibitors through the fit of the slopes obtained by the double reciprocal plot. As shown in Fig. 3, the inhibitor **JMM-2** showed a K_i calculated for G6P of 142 μM , while that for the NADP⁺ substrate was 228 μM (Fig. 3A). The inhibitor **CCM-4** showed K_i values of 101 μM and 42 for G6P and NADP⁺, respectively (Fig. 3B). In addition, the inhibitors **CNZ-7** and **CNZ-3** showed similar K_i values to the G6P substrate of 223 μM and 206 μM , respectively, while for the NADP⁺ substrate, the K_i values were 47 μM and 134 μM for the inhibitors **CNZ-7** and **CNZ-3**, respectively (Fig. 3C–D). These results are in accordance with the mechanism of action determined for the four inhibitors because an alteration in G6PD activity was observed in all the compounds when the concentrations of the inhibitors were increased. Finally, it is interesting to note that the **CCM-4** inhibitor showed better HsG6PD enzyme binding affinity, while the **JMM-2** inhibitor showed less affinity for binding with the ES complex for the G6P substrate (142 μM) with respect to the NADP⁺ substrate (228 μM).

Finally, in Table 2, we show a summary of the biochemical parameters determined for the four-hit compounds. As is evident, the **CNZ-3**

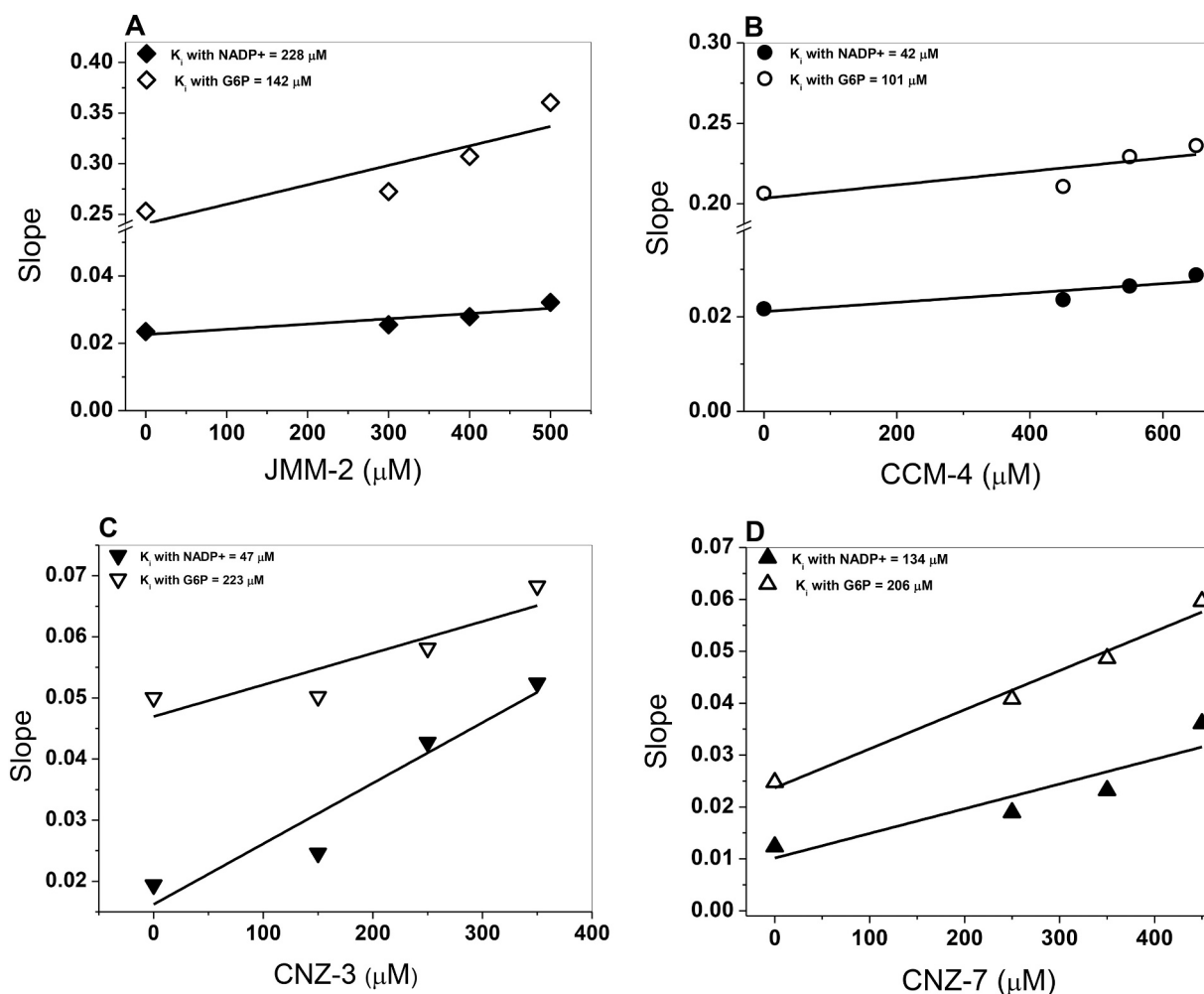


Fig. 3. Determination of K_i value. The slope values were calculated by fitting K_m or V_{\max} versus the compound concentrations of (A) **JMM-2**, (D) **CCM-4**, (B) **CNZ-3**, and (C) **CNZ-7**. The data represent the mean of three independent experiments.

Table 2

Summary of the constants and types of inhibition obtained from the compounds analyzed in this study.

Inhibitor	Inhibition (%)	IC ₅₀ (μM)	k ₂ (M ⁻¹ s ⁻¹)	Inhibition type		K _i (μM)	
				G6P	NADP ⁺	G6P	NADP ⁺
JMM-2	89.5	307	0.50	NC	NC	142	228
CCM-4	47.3	412	0.63	UC	UC	101	42
CNZ-3	92.6	121	0.66	NC	UC	223	47
CNZ-7	68.0	274	0.83	UC	UC	206	134
Without	–	–	–	–	–	38.5*	6.1*

NC = noncompetitive inhibition. UC = uncompetitive inhibition.

* K_m without inhibitor.

compound showed the best inactivation in the HTS assay and showed better second-order inactivation constants (k_2), indicating that this compound represents the best rate of formation of the enzyme-inhibitor complex with the HsG6PD enzyme, but it does not bind at the same site as the substrates, and probably CNZ-3 competes near to NADP⁺ binding site as indicated by the inhibition type assay, where we observed that the K_m value for NADP⁺ increases, so CNZ-3 presents a higher K_i value concerning the other three compounds.

3.2. Structural studies of the HsG6PD enzyme with inhibitory compounds

3.2.1. Circular dichroism (CD) and thermal stability assays

To analyze the effect of inhibitors on the secondary structure of the HsG6PD protein, circular dichroism (CD) assays were performed in the presence of the IC₅₀ concentration after incubating the enzyme with each of the inhibitors. All spectra of HsG6PD with the inhibitors showed minimum absorption peaks at 208 nm and 222 nm corresponding to β-sheets and α-helices. Nevertheless, as shown in Fig. 4A, when the HsG6PD protein was incubated with the inhibitors, differences were observed in the minimum absorption signals with respect to the HsG6PD enzyme without an inhibitor. The inhibitor that most altered the

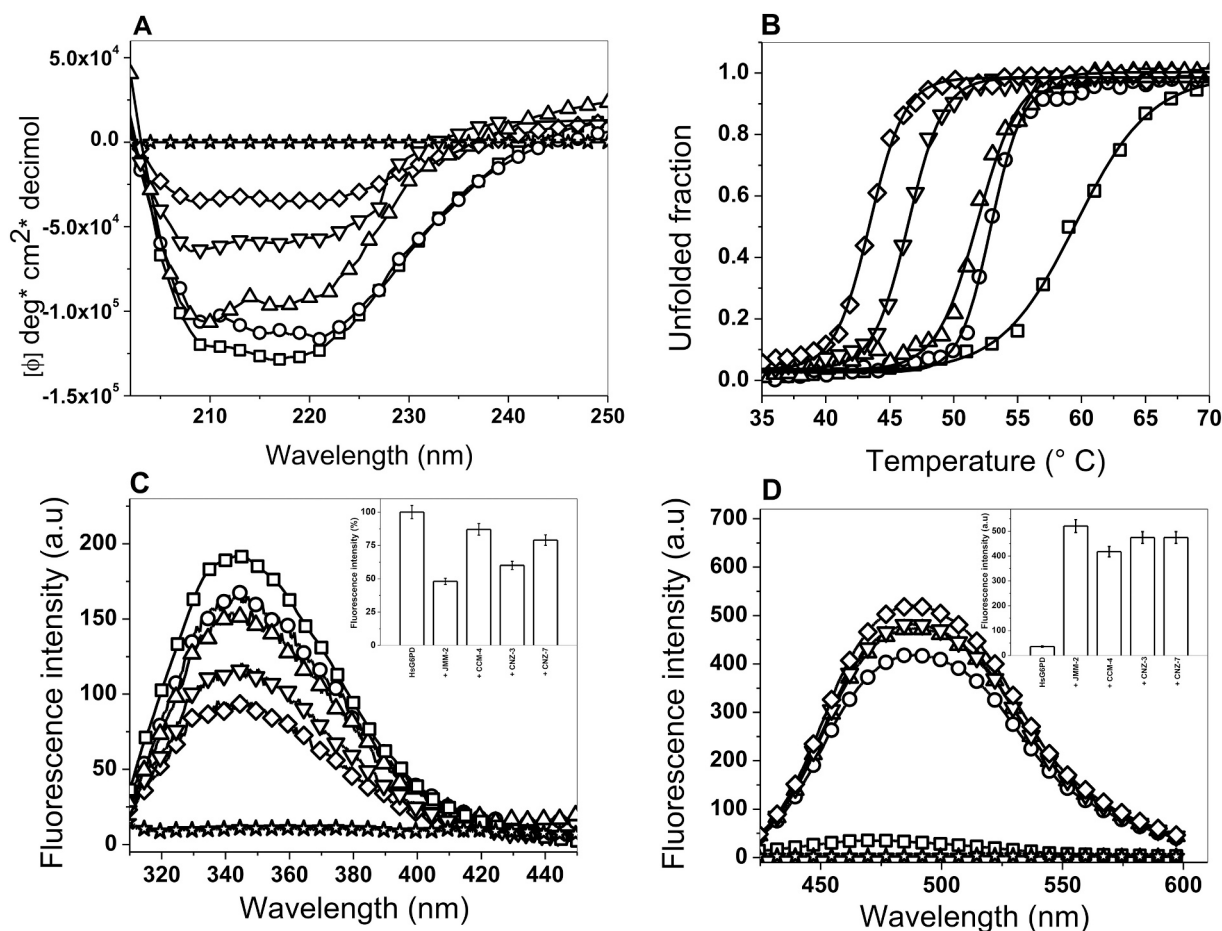


Fig. 4. Spectroscopic characterization of recombinant HsG6PD protein in the absence (□) and presence of the four inhibitors (◇) JMM-2, (○) CCM-4, (▽) CNZ-3, and (Δ) CNZ-7 chemical compounds. (A) Far-UV circular dichroism (CD) spectra of HsG6PD. (B) Thermal stability of the HsG6PD protein. (C) Intrinsic fluorescence spectra of the HsG6PD enzyme. Inset: Intrinsic fluorescence obtained by subtracting the blank from the values of total fluorescence intensity. The HsG6PD free of compounds was fixed as 100%. (D) 8-Anilino-1-naphthalene-1-sulfonate (ANS) assays of the HsG6PD enzyme. Inset: ANS fluorescence obtained by subtracting the blank (ANS without protein; open stars) from the values of total fluorescence intensity. In all the assays, the protein was incubated for 2 h at 37 °C prior to measurement. The experiments were performed in triplicate. The experimental conditions for all the experiments are described in the Materials and Methods section.

secondary structure was **JMM-2** because it had a spectrum closer to the blank, while the **CNZ-3** inhibitor was the second most effective compound in terms of altering the secondary structure of the HsG6PD protein. Finally, the two inhibitors that altered the secondary structure to a lesser extent were the **CNZ-7** and **CCM-4** inhibitors. These results indicate that all compounds affect the secondary structure of HsG6PD, which explains the loss of catalytic activity and is in accordance with those observed in biochemical assays, where it was detected that the chemical compounds **JMM-2** and **CNZ-3** showed the best inhibitory activity on the HsG6PD protein.

Because the inhibitors reduce the catalytic activity and alter the secondary structure of the HsG6PD protein, it was necessary to evaluate the effect on thermal stability (T_m) after incubation with the four inhibitors following changes in the CD signal at 222 nm. Important features were observed for the enzyme-free inhibitors and in the presence of inhibitors, as shown in Fig. 4B. The T_m calculated for the enzyme-free inhibitors was 59.6 °C, while the inhibitors induced an evident decrease (minus 7–16 °C) in the T_m values of HsG6PD. The enzyme was most affected in the presence of the **JMM-2** inhibitor with a decrease of 16 °C in thermal stability (T_m value of 43.4 °C), while the **CNZ-3** inhibitor showed a decrease of 13 °C in terms of thermal stability (T_m value of 46.5 °C) with respect to the inhibitor-free enzyme. In contrast, the inhibitors **CNZ-7** and **CCM-4** showed decreases of 7.8 °C and 6.7 °C (T_m values of 51.8 °C and 52.9 °C), respectively. These data confirm that the four inhibitors have a strong effect on the global stability of the HsG6PD protein in addition to their effects on catalysis and loss of secondary structure.

3.2.2. Intrinsic and extrinsic fluorescence assays

Finally, because of the inhibitors altering the secondary structure and the global stability of the HsG6PD protein, we performed intrinsic and extrinsic fluorescence assays to determine the changes in the tertiary structure of the protein. The intrinsic fluorescence of the seven tryptophan residues contained in the HsG6PD/monomer was monitored to determine structural changes in the presence of the four inhibitors. We found that the intrinsic fluorescence for the native HsG6PD protein without inhibitors showed a peak at 344 nm with a maximum intensity of 191 arbitrary units (a.u.) (Fig. 4C), while the presence of the inhibitors induced a reduction in the maximum peak of fluorescence: 12%–51% of the signal was lost in the presence of the inhibitors (Fig. 4C. Inset). Compared to the absence of inhibitor, the inhibitor that induced the largest changes in the tertiary structure of the protein was **JMM-2** because the maximum intensity of fluorescence decreased by 51% (93 a.u.) (Fig. 4C), while the inhibitor **CNZ-3** was the second most effective inhibitor in terms of inducing alterations in the tertiary structure of the protein, where the maximum intensity of fluorescence was reduced by 40% (115.82 a.u.). Finally, the inhibitors **CNZ-7** (151 a.u.) and **CCM-4** (167 a.u.) induced fewer alterations in the tertiary structure of the protein, where reductions of 21% and 12%, respectively, were observed (Fig. 4C). As previously noted, the decrease in fluorescence intensity could be because seven tryptophan residues were exposed to the environment after incubation with the inhibitors, inducing the unfolding of the native three-dimensional (3D) structure, which caused a negative effect on the activity of HsG6PD. Furthermore, these results are again related to the grade of inhibition that each molecule shows toward HsG6PD as well as the alteration in the secondary structure and the global stability of the HsG6PD protein.

In addition, we used a fluorescent molecular probe (extrinsic fluorescence) as another form to corroborate the alterations in the 3D structure of the HsG6PD protein. To identify possible structural changes, we monitored the fluorescence of ANS with HsG6PD in the presence of the four inhibitors. The ANS molecule has a high affinity for hydrophobic regions; therefore, inhibitors that alter the 3D structure of the HsG6PD protein to a greater extent will contain more hydrophobic regions and will exhibit higher ANS fluorescence signals. As seen in Fig. 4D, all maximum extrinsic fluorescence intensities obtained for

HsG6PD in the presence of the four inhibitors were higher than those obtained for the enzyme without an inhibitor. The HsG6PD enzyme without an inhibitor has a maximal fluorescence emission spectrum of 36 a.u., while compared with the control, HsG6PD incubated with **JMM-2** produced an ANS spectrum with maximal fluorescence at 486 nm with 521 a.u. and an increase of 14.8-fold in fluorescence intensity was observed. Furthermore, the emission spectrum of the HsG6PD enzyme incubated with the inhibitors **CNZ-3** and **CNZ-4** showed similar maximum intrinsic fluorescence intensities of approximately 475 a.u., whereas compared to the control, a 13.5-fold increase in fluorescence intensity was observed (Fig. 4D. Inset). Finally, compared to HsG6PD without an inhibitor, the chemical inhibitor that presented the least intensity of extrinsic fluorescence was **CCM-4** (418 a.u.) with an 11.8-fold increase, which indicates that this last compound was the one that caused the fewest alterations in the 3D structure of the human G6PD protein. Thus, the increase in fluorescence intensity by more than 11.8-fold to 14.8-fold in the HsG6PD enzyme in the presence of the inhibitors indicated that ANS found more buried hydrophobic pockets in the HsG6PD enzyme in the presence of the four inhibitors.

3.3. Molecular docking

For the molecular docking study, the most active compounds **JMM-2** and **CNZ-3** were selected because they first showed noncompetitive inhibition for both substrates and **CNZ-3** showed noncompetitive inhibition for G6P and uncompetitive inhibition for NADP⁺. We performed blind molecular docking over the entire protein. To help us understand the observed experimental activities, molecular docking studies were carried out using Auto Dock Vina software to obtain the plausible binding mode of the studied compounds. In addition, this was used to deepen our understanding of the interaction between selected hits and HsG6PD. In Fig. 5, the in silico study revealed four zones of interaction for the **JMM-2** compound (Fig. 5A). In general, 70% of the poses obtained in the whole docking experiment had to be repeated in the same pocket of HsG6PD that was localized far from the active site and very close to the structural NADP⁺ binding site (zone 3) (Fig. 5A), which is involved in the dimerization and stability of the enzyme [35]. The most stable protein-ligand complex showed a $\Delta G = -6.91 \pm 0.09$ kcal/mol. In addition, in zone 3, we observed that phenylpropionic acid showed two H-bond interactions with Asn229 and Asn288 and fifteen nonpolar contacts. Furthermore, the biphenyl moiety showed π - π interactions with Phe221 and Phe373 (Fig. 5B).

With respect to the docking predicted with **CNZ-3**, the in silico study also revealed four main zones of interaction, as shown in Fig. 5C (Zones 1–4), and an increase in the formation of hydrogen bridges concerning **JMM-2** was observed. In zone 1, the protein-ligand interaction showed that **CNZ-3** bound very close to the active site of HsG6PD and interacted with Gln-83 by one H-bond, and nine nonpolar contacts were found (Fig. 5D). The most stable protein-ligand complex in zone 1 showed an affinity energy of -5.99 ± 0.03 Kcal/mol. Zone 2 was located near the binding of G6P in the active site, and **CNZ-3** possesses the ability to form one H-bond with Leu433 and nine nonpolar contacts, where the most stable protein-ligand complex showed a $\Delta G = -7.51 \pm 0.09$ kcal/mol (Fig. 5E). With respect to zone 3, we found that **CNZ-3** possesses the ability to bind a pocket localized very close to the structural NADP⁺ binding site by a H-bond with Arg487, and eight nonpolar contacts were found ($\Delta G = -6.91 \pm 0.02$ kcal/mol) (Fig. 5F). It is interesting to note that **CNZ-3** probably enters the structural NADP⁺ binding site because **CNZ-3** interacts with 5 of the 12 amino acids (Arg487, Arg370, Tyr401, Lys403, and Tyr503) that participate in the binding of structural NADP⁺. Finally, the zone with the most interactions by hydrogen bridges was zone 4 (Fig. 5G), where five H-bonds with Glu244, Lys320, Gly321 (2 hydrogen bonds), and Tyr308 were observed. Furthermore, we observed eight nonpolar contacts, and the most stable protein-ligand complex showed a $\Delta G = -6.53 \pm 0.03$ kcal/mol. This pocket was localized far from the active site and the structural NADP⁺ binding site.

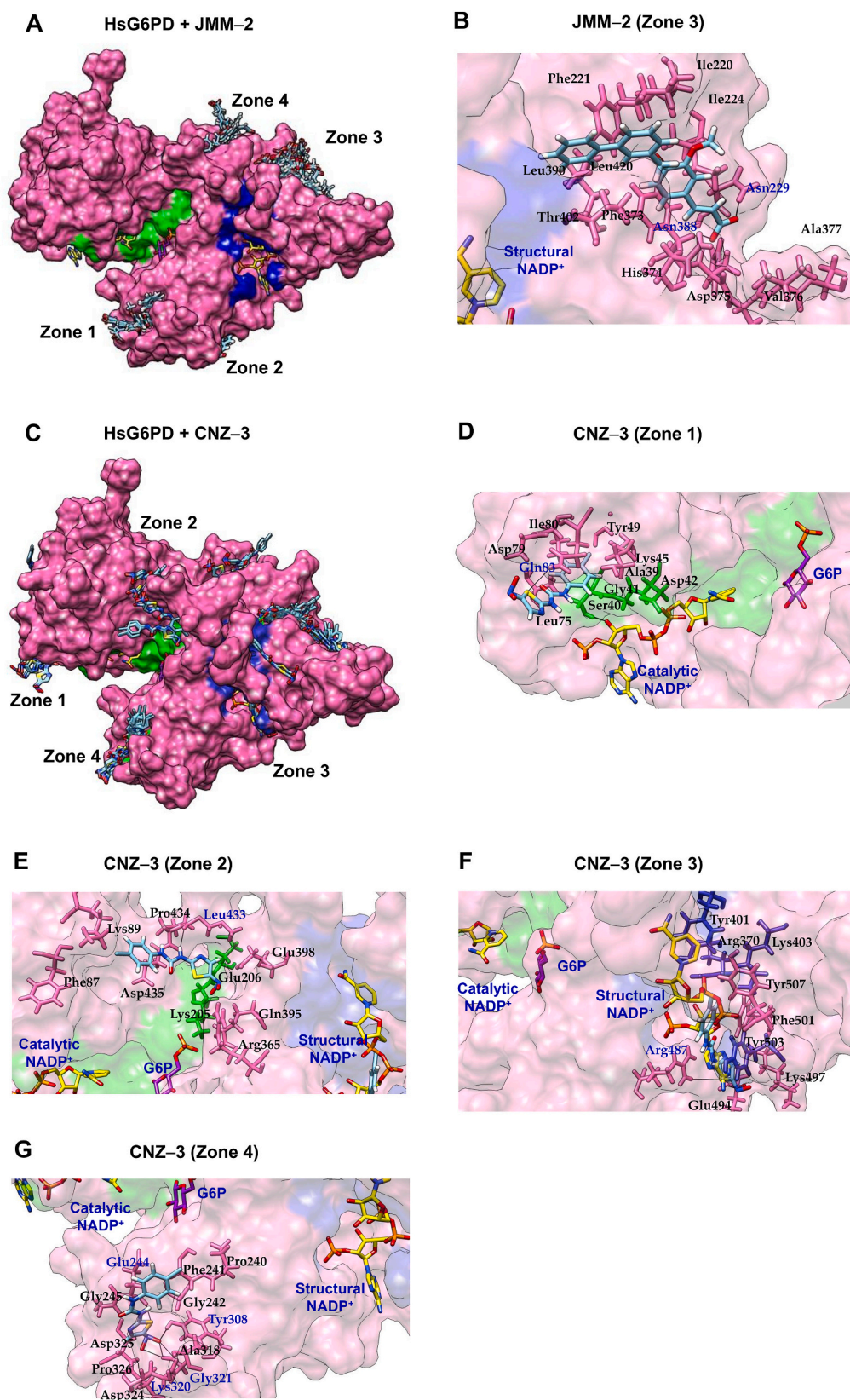


Fig. 5. Molecular docking of compounds **JMM-2** and **CNZ-3** on HsG6PD (PDB 2BHL). (A) A general view of the binding affinities of **JMM-2** with the HsG6PD protein. (B) Zoom of the interaction of zone 3 with **JMM-2** on the HsG6PD structure, showing amino acids involved in the binding pocket with the compound. (C) A general view of the binding affinities of **CNZ-3** with the HsG6PD protein. (D) Zoom of zone 1 with the interactions of **CNZ-3** in the HsG6PD structure, showing amino acids involved in the binding pocket near the catalytic site NADP⁺. (E) Zoom of zone 2, showing amino acids of interaction near the catalytic site. (F) Zoom of zone 3, showing amino acids involved in the binding pocket near the structural site NADP⁺. (G) Zoom of zone 4, showing amino acids of interaction with **CNZ-3**. The interactions are shown in black.

4. Discussion

The pentose phosphate pathway (PPP) has been proposed to play a crucial role in cancer cells, as it has been associated with increased HsG6PD activity [13,22,36]. Because of the important role of HsG6PD activity in cancer cells, various mechanisms have been developed to inhibit the catalytic activity of this enzyme to decrease the nucleotide precursors involved in proliferation, as well as inhibit NADPH, which is used for both intracellular ROS detoxification and catabolic metabolism.

For the above, in this work, we identified four molecules that inhibited HsG6PD by more than 40%, named **JMM-2**, **CCM-4**, **CNZ-3**, and **CNZ-7**. The compounds **CNZ-3** and **CNZ-7** are derivatives of nitazoxanide; in another study, it was shown that these compounds have trichomonacidal and antileishmanial activity [37]. Then, an orthogonal assay was performed to obtain the IC_{50} values of the four compounds. The most effective compound was **CNZ-3** ($IC_{50} = 121 \mu M$) (Fig. 6), which inactivated the enzyme at lower concentrations than the other compounds tested, including 1-dehydroepiandrosterone (DHEA), which has been used as an inhibitor of the HsG6PD enzyme, showing an IC_{50} of $483 \mu M$ [26].

The second-order inactivation constant k_2 was used to determine the ratio formation of the complex enzyme inhibitor with the HsG6PD enzyme. Our results showed that **CNZ-7** had the best k_2 , which indicates that the inhibitor **CNZ-7** bound faster with the HsG6PD enzyme to form the enzyme-inhibitor complex and therefore inactivated the enzyme. It is important to note that there is no study on G6PD inhibitors in which the k_2 values of each of the inhibitors have been calculated.

Kinetic characterization studies revealed that the four compounds inhibited the HsG6PD enzyme by noncompetitive and uncompetitive type inhibition, while Preuss et al. [26] reported competitive inhibition for their four analyzed compounds, including DHEA and 6AN inhibitors of the HsG6PD enzyme. In addition, we determined the inactivation

constants (K_i) for the four inhibitors and observed that all the inhibitors have different affinities for binding with HsG6PD. **CCM-4** was the inhibitor with the best affinity, with a K_i value of $42.6 \mu M$, followed by the inhibitor **JMM-2**, with a K_i value of $142 \mu M$ (Fig. 6).

To demonstrate that the effect of inhibitors not only occurs at the functional level but could also occur at the structural level, we evaluated the effect of the four inhibitors on the secondary structure of the HsG6PD protein by circular dichroism (CD) assay. **JMM-2** and **CNZ-3** were the inhibitors that most altered the secondary structure, followed by the inhibitors **CNZ-7** and **CCM-4**. These results indicate that all the compounds affect the secondary structure of HsG6PD, which explains the loss of catalytic activity. In addition, we evaluated the effect of the four inhibitors on the thermal unfolding stability (T_m) of the HsG6PD protein and found that compared to the enzyme without an inhibitor, the enzyme was strongly perturbed at the structural level by all the inhibitors. The inhibitors that most perturbed the enzyme were **JMM-2** and **CNZ-3**, where a decrease of $16^\circ C$ and $13^\circ C$ of thermal stability was observed. These data confirm that the four inhibitors also have a strong effect on the conformational stability of the HsG6PD protein (Fig. 6).

Additionally, we found that compared to that without the inhibitor, the intrinsic fluorescence of the native HsG6PD protein in the presence of the four inhibitors induced a reduction in the maximum peak fluorescence intensity from 12% to 51%. These results again suggest that the inhibitors affect the native 3D structure of the protein. In addition, the fluorescence of the ANS probe was more than 14-fold higher in the presence of the inhibitors, indicating that compared to the control enzyme, ANS interacted with more exposed hydrophobic sites in the HsG6PD enzyme in the presence of the four inhibitors (Fig. 6). It is important to mention that this is the first time structural alterations of HsG6PD have been studied in the presence of inhibitors.

Regarding the docking predicted with the compound **JMM-2**, we observed that 70% of the poses were obtained in the pocket far from the

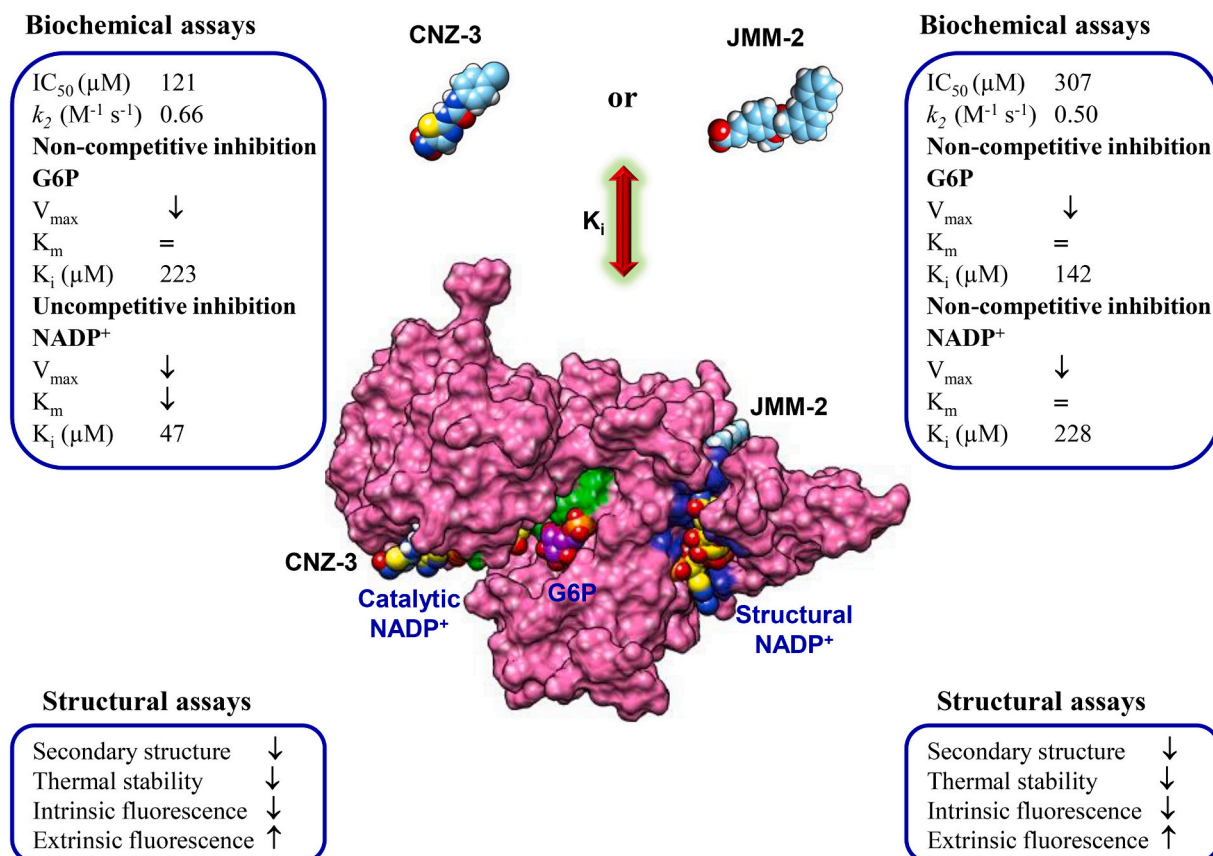


Fig. 6. Summary of the effects of **JMM-2** and **CNZ-3** compounds on HsG6PD protein at biochemical and structural levels.

active site and close to the structural NADP⁺ binding site with two H-bond interactions. This result is in agreement with the one observed in the inhibition assay, where the compound **JMM-2** showed noncompetitive-type inhibition for G6P and NADP⁺ substrates, indicating that the compound bound to a place other than the active site, meaning that affinity was not affected, but the rate at which the enzyme-catalyzed the reaction was affected, which was probably due to a conformational change caused by the union of **JMM-2** to the enzyme to form the inhibitor-enzyme complex (Fig. 6). In addition, **JMM-2** was the inhibitor that most altered the secondary structure and thermal stability and induced the largest changes in the tertiary structure of HsG6PD. These results are in concordance with those observed in the molecular blind docking analysis, where the stable protein-**JMM-2** complex was localized close to the structural NADP⁺ binding site in the HsG6PD enzyme, which has been proposed to be crucial for the long-term stability of the enzyme and stabilization of the dimer state [38].

Finally, we observed four interaction zones of HsG6PD in the blind molecular docking with compound **CNZ-3**. Zone 1 was located near the active site of the HsG6PD protein and interacts by nonpolar contacts with Ala39, Ser40, Gly41, Asp42, and Lys45, which belong to a conserved fragment nucleotide-binding fingerprint 38-GxxGGDLA-44 involved in the binding of NADP⁺ coenzyme. This result is in concordance with the previously observed inhibition type for the NADP⁺ substrate, where the inhibition was uncompetitive type, while that in zone 2, **CNZ-3** was located near the binding site G6P substrate and interacted by nonpolar contacts with Lys205 and Glu206, where Lys205 is the amino acid responsible for substrate binding and catalysis in the HsG6PD enzyme. These results could indicate that the binding of **CNZ-3** near the active site is in agreement with the previously observed noncompetitive-type inhibition of the G6P substrate because the V_{\max} decreased, but the K_m was not influenced (Fig. 6). Regarding zone 3, **CNZ-3** binds a pocket localized very close to the structural NADP⁺ binding site, and nonpolar contacts interact with Arg370, Tyr401, Lys403 and Tyr503, which are involved in the binding of structural NADP⁺. It is interesting to note that **CNZ-3** was the second most effective compound in terms of altering the secondary structure, thermal stability (loss of 13 °C in terms of the T_m value in the absence of the compound) and alterations in the tertiary structure of the HsG6PD protein. In addition, various working groups have observed that mutations in HsG6PD that occur near the structural NADP⁺ binding site decrease the catalytic activity, stability and dimerization of the enzyme [3–5,34,38,39].

It is interesting to note that all the results shown in this work indicate that the HsG6PD protein shows alterations in the activity, secondary structure, global stability, and changes in the tertiary structure of the protein when the protein was incubated with the inhibitors (Fig. 6). In addition, it is important to note that this is the first report in which alterations of the secondary and 3D structure of the HsG6PD protein are reported in the presence of inhibitors.

5. Conclusions

In this study, four new synthetic inhibitors (**JMM-2**, **CCM-4**, **CNZ-3**, and **CNZ-7**) and their effect on HsG6PD activity and structure were studied. These new inhibitors showed a higher percentage of inhibition, altered the secondary structure and thermal unfolding stability and affected the native three-dimensional (3D) structure of the protein. In addition, the mechanisms of inhibition were noncompetitive and uncompetitive. This type of inhibition is important in the search for drugs since the compounds under study do not compete to bind to the active center of the enzyme, which in terms of dose effect, would be equivalent to using low doses of the compound to achieve the desired effect. The new inhibitors of HsG6PD presented in this work are potential candidates for future in vitro studies in several human antitumor therapies since HsG6PD is a key enzyme in the PPP, a pathway that cancer cells in proliferating use to cover both the nucleotide precursors needed for

proliferation and NADPH, a fundamental molecule for the synthesis of fatty acids, which are essential in the synthesis of cell membranes.

Funding

This research was funded by the E022 Program, National Institute of Pediatrics, Mexico City, Mexico (Recursos Fiscales para la Investigación). SGM. was supported by INP 031/2018. JM.Q. was supported by INP 024/2017 and CONACYT grant 259201, Cátedras CONACYT (2184), project number 2057. BHO is supported by HIM/2017/100.

Inform consent

Not applicable.

Ethical approval

This article does not contain any studies with human participants performed by any of the authors. Research involving Human Participants and/or Animals: In this study, there isn't any research involving Human participant or animals.

Declaration of Competing Interest

The authors declare that they have no conflicts of interest with the contents of this article.

Acknowledgments

E.J.R.-N, B.H.-O, V.M.-R, and L.M.-L thank the CONACYT fellowship for the financial support. The technical assistance of Camila Marcial, Ximena Gomez-Gonzalez, and Maria Jose Gomez-Gonzalez is greatly appreciated. Finally, we thank Javier Gallegos Infante (Instituto de Fisiología Celular, UNAM) for assistance with the bibliographic materials.

References

- [1] N. Hamilton, M. Dawson, E. Fairweather, N.S. Hitchin, D. James, S. Jones, A. Jordan, A. Lyons, H. Small, G. Thomson, I. Waddell, D. Ogilvie, Novel steroid inhibitors of Glucose-6-phosphate dehydrogenase, *J. Med. Chem.* 55 (2012) 4431–4445.
- [2] D. Cappellini, G. Fiorelli, Glucose-6-phosphate dehydrogenase deficiency, *Lancet.* 606 (2008) 67–74.
- [3] S. Gómez-Manzo, J. Terrón-Hernández, I. De la Mora-De la Mora, A. González-Valdez, J. Marcial-Quino, I. García-Torres, A. Vanoye-Carlo, G. López-Velázquez, G. Hernández-Alcantara, J. Oria-Hernández, H. Reyes-Vivas, S. Enríquez-Flores, The stability of G6PD is affected by mutations with different clinical phenotypes, *Int. J. Mol. Sci.* 15 (2014) 21179–21201.
- [4] S. Gómez-Manzo, J. Marcial-Quino, A. Vanoye-Carlo, S. Enríquez-Flores, I. De la Mora-De la Mora, A. González-Valdez, I. García-Torres, V. Martínez-Rosas, E. Sierra-Palacios, F. Lazcano-Pérez, E. Rodríguez-Bustamante, R. Arreguin-Espinosa, Mutations of glucose-6-phosphate dehydrogenase durham, Santa-Maria and A+ variants are associated with loss functional and structural stability of the protein, *Int. J. Mol. Sci.* 16 (2015) 28657–28668.
- [5] S. Gómez-Manzo, J. Marcial-Quino, A. Vanoye-Carlo, H. Serrano-Posada, A. González-Valdez, V. Martínez-Rosas, B. Hernández-Ochoa, E. Sierra-Palacios, R. A. Castillo-Rodríguez, M. Cuevas-Cruz, E. Rodríguez-Bustamante, R. Arreguin-Espinosa, Functional and biochemical characterization of three recombinant human Glucose-6-Phosphate Dehydrogenase mutants: Zacatecas, Vanua-Lava and Viangchan, *Int. J. Mol. Sci.* 17 (2016) 787.
- [6] A. Fico, F. Paglialunga, L. Cigliano, P. Abrescia, P. Verde, G. Martini, L. Laccarino, S. Filosa, Glucose-6-phosphate dehydrogenase pays a crucial role in protection from redox-stress-induced apoptosis, *Cell Death Differ.* 11 (2014) 823–831.
- [7] P. Jiang, W. Du, M. Wu, Regulation of the pentose phosphate pathway in cancer, *Protein & Cell.* 5 (8) (2014) 592–602.
- [8] S. Eunae, H. Yong, K. Hyun, K. Nam, Y. Jong, The pentose phosphate pathway as a potential target for Cancer therapy, *Biomolecules & Theapeutics.* 26 (1) (2018) 29–38.
- [9] N.S. Rajasekaran, P. Connel, E.S. Christians, L.J. Yan, R.P. Taylor, A. Orosz, X. Q. Zhang, T.J. Stevenson, R.M. Peshok, J.A. Leopold, W.H. Barry, Human α B-crystallin mutation causes oxidoreductive stress and protein aggregation cardiomyopathy in mice, *Cell.* 130 (2007) 427–439.

- [10] R.S. Gupte, V. Vijay, B. Marks, R.J. Levine, H.N. Sabbah, M.S. Wolin, F.A. Recchia, S.A. Gupte, Upregulation of glucose-6-phosphate dehydrogenase and NAD(P)H oxidase activity increases oxidative stress in failing human heart, *J Card Fail.* 13 (2007) 497–506.
- [11] K. Patra, N. Hay, The pentose phosphate pathway and cancer, *Cell Press.* 39 (2014) 347–354.
- [12] D. Catanzaro, E. Gaude, G. Orso, C. Giordano, G. Guzzo, A. Rasola, R. Eugenio, L. Caparrotta, C. Frezza, M. Mantopoli, Inhibition of glucose-6-phosphate dehydrogenase sensitizes cisplatin-resistant cells to death, *Oncotarget.* 6 (2015) 30.
- [13] C. Riganti, E. Gazzano, M. Polimeni, E. Aldieri, D. Ghigo, The pentose phosphate pathway: an antioxidant defense and a crossroad in tumor cell fate, *Free Radic. Biol. Med.* 53 (2012) 421–436.
- [14] W. Yang, L. Yen, S. Hwang, The redox role of G6PD in cell growth, cell death, and Cancer, *Cells.* 8 (2019) 1055.
- [15] I. Giacomini, E. Ragazzi, G. Pasut, M. Montopoli, The pentose phosphate pathway and its involvement in cisplatin resistance, *Int. J. Mol. Sci.* 21 (2020) 937.
- [16] C.L. Liu, Y.C. Hsu, J.J. Lee, M.J. Chen, C.H. Lin, S.Y. Huang, S.P. Cheng, Targeting the pentose phosphate pathway increases reactive oxygen species and induces apoptosis in thyroid cancer cells, *Mol Cell Endocrinol.* 499 (2020) 110595.
- [17] K. Duvel, J.L. Yecies, S. Menon, P. Raman, A.L. Lipovsky, A.L. Souza, E. Triantafellow, Q. Ma, R. Gorski, S. Cleaver, Activation of a metabolic gene regulatory network downstream of mTOR complex 1, *Mol. Cell* 39 (2010) 171–183.
- [18] W. Du, P. Jian, A. Manuso, A. Stonestrom, M.D. Brewer, A.J. Minn, T.W. Mak, X. Yang, Tap73 enhances the pentose phosphate pathway and supports cell proliferation, *Nat. Cell Biol.* 15 (2013) 991–1000.
- [19] A. Wagle, S. Jivraj, G.L. Garlock, S.R. Stapleton, Insulin regulation of glucose-6-phosphate dehydrogenase gene expression in rapamycin-sensitive and requires phosphatidylinositol 3-kinase, *J. Biol. Chem.* 273 (1998) 14968–14974.
- [20] X. Hong, R. Song, H. Song, T. Zheng, J. Wang, Y. Liang, S. Qi, Z. Lu, X. Song, H. Jiang, PTEN antagonizes Tc1/hnRNP-mediated G6PD pre-mRNA splicing which contributes to hepatocarcinogenesis, *Gut.* 63 (2014) 1637–1647.
- [21] C. Cosentino, D. Grieco, V. Costanzo, ATM activates the pentose phosphate pathway promoting anti-oxidant defence and DNA repair, *EMBO J.* 30 (2010) 546–555.
- [22] P. Jiang, W. Du, M. Wu, Regulation of the pentose phosphate pathway in cancer, *Protein & Cell.* 5 (8) (2014) 592–602.
- [23] O.H. Minchenko, I.A. Garmash, D.O. Minchenko, A.Y. Kuznetsova, O.O. Ratushna, Inhibition of IRE1 modifies hypoxic regulation of G6PD, GPI, TKT, TALDO1, PGLS and RPIA genes expression in U87 glioma cells, *Ukr Biochem J.* 89 (1) (2017) 38–49.
- [24] S. Langbein, W. Frederiks, A. Hausen, J. Popa, J. Lehmann, C. Weiss, P. Alken, J. Coy, Metastasis is promoted by a bioenergetics switch: new targets for progressive renal cell cancer, *Int. J. Cancer* 122 (2008) 2422–2428.
- [25] S.A. Grupte, Glucose-6-phosphate dehydrogenase: a novel therapeutic target in cardiovascular diseases, *Curr Opin Investg Drugs.* 9 (2008) 993–1000.
- [26] J. Preuss, A.D. Richardson, A. Pinkerton, M. Hedrick, E. Sergienko, S. Rahlfs, K. Becker, L. Bode, Identification of novel human Glucose-6-phosphate dehydrogenase inhibitors, *J Biom Screening.* 18 (2013) 286–297.
- [27] S. Devan, V.A. Janardhanam, Effect of Naringenin on metabolic markers, lipid profile and expression of GFAP in C6 glioma cells implanted rat's brain, *Ann. Neurosci.* 18 (4) (2011) 151–155.
- [28] F. Leonardi, L. Attorri, R. Di Benedetto, A. Di Biase, M. Sanchez, M. Nardini, S. Salvati, Effect of arachidonic, eicosapentaenoic and docosahexaenoic acids on the oxidative status of C6 glioma cells, *Free Radic. Res.* 39 (8) (2005) 865–874.
- [29] H.D. Panchal, K. Vranizan, C.Y. Lee, J. Ho, J. Ngai, P.S. Timiras, Early anti-oxidative and anti-proliferative curcumin effects on neuroglioma cells suggest therapeutic targets, *Neurochem. Res.* 33 (9) (2008) 1701–1710.
- [30] C.A. Yang, H.Y. Huang, C.L. Lin, J.G. Chang, G6PD as a predictive marker for glioma risk, prognosis and chemosensitivity, *J. Neuro-Oncol.* 139 (3) (2018) 661–670.
- [31] I. Garcia-Torres, I. De, La Mora- De La Mora, J. Marcial-Quino, S. Gómez-Manzo, A. Vanoye-Carlo, G. Navarrete-Vázquez, B. Colín-Lozano, P. Gutiérrez-Castrellón, E. Sierra-Palacios, G. López-Velázquez, S. Enríquez-Flores, Protom pump inhibitors drastically modify triosephosphate isomerase from *Giardia lamblia* at functional and structural levers, proving molecular leads in the desing of new anti-giardiasis drugs, *Biochim. Biophys. Acta* (2016) 97–107.
- [32] B. Hernández-Ochoa, G. Navarrete-Vázquez, C. Nava-Zuazo, A. Castillo-Villanueva, S.T. Méndez, A. Torres-Arroyo, S. Gómez-Manzo, J. Marcial-Quino, M. Ponce-Macotela, Y. Rufino-Gonzalez, M. Martínez-Gordillo, G. Palencia-Hernández, N. Esturau-Escofet, E. Calderon-Jaimes, J. Oria-Hernández, H. Reyes-Vivas, Novel giardicidal compounds bearing proton pump inhibitor scaffold proceeding through triosephosphate isomerase inactivation, *Sci. Rep.* 7 (2017) 7810.
- [33] E.J. Ramírez-Nava, D. Ortega-Cuellar, A. González-Valdez, R.A. Castillo-Rodríguez, G.Y. Ponce-Soto, B. Hernández-Ochoa, N. Cárdenas-Rodríguez, V. Martínez-Rosas, L. Morales-Luna, H. Serrano-Posada, E. Sierra-Palacios, R. Arreguin-Espinosa, M. Cuevas-Cruz, L.M. Rocha-Ramírez, V. Pérez de la Cruz, J. Marcial-Quino, S. Gómez-Manzo, Molecular Cloning and Exploration of the Biochemical and Functional Analysis of Recombinant Glucose-6-Phosphate Dehydrogenase from *Gluconoacetobacter diazotrophicus* PAL5, *Int J Mol Sci.* 24 (2019) 20–21.
- [34] Y.Y. Cortés-Morales, A. Vanoye-Carlo, R.A. Castillo-Rodríguez, H. Serrano-Posada, A. González-Valdez, D. Ortega-Cuellar, B. Hernández-Ochoa, L.M. Moreno-Vargas, D. Prada-Gracia, E. Sierra-Palacios, Cloning and biochemical characterization of three glucose 6 phosphate dehydrogenase mutants presents in the Mexican population, *Int. J. Biol. Macromol.* 119 (2018) 926–936.
- [35] M. Kotaka, S. Gover, L. Vandeputte-Rutten, S.W.N. Au, V.M.S. Lam, M.J. Adams, Structural studies of glucose-6-phosphate and NADP⁺ binding to human glucose-6-phosphate dehydrogenase, *Acta Crystallogr. D* 61 (2005) 495–504.
- [36] L. Mele, F. Paino, F. Papaccio, T. Regad, D. Boocock, P. Stiuss, A. Lombardi, D. Liccardo, G. Aquino, A. Barbien, C. Arra, C. Coveney, M. La Noce, G. Papaccio, M. Caraglia, C. Tirini, V. Desiderio, A new inhibitor of glucose-6-phosphate dehydrogenase blocks pentose phosphate pathway and suppresses malignant proliferation and metastasis in vivo, *Cell Death and Disease* 9 (2018) 572.
- [37] C. Nava-Zuazo, F. Chávez-Silva, R. Moo-Puc, M.J. Chan-Bacab, B.O. Ortega-Morales, H. Moreno-Díaz, D. Díaz-Coutiño, E. Hernández-Nuñez, G. Navarrete-Vázquez, 2-Acylamino-5-nitro-1,3-thiazoles: preparation and in vitro bioevaluation against four neglected protozoan parasites, *Bioorg. Med. Chem.* 22 (2014) 1626–1633.
- [38] X.T. Wang, T.F. Chan, V.M. Lam, P.C. Engel, What is the role of the second "structural" NADP⁺-binding site in human glucose 6-phosphate dehydrogenase? *Protein Sci.* 17 (8) (2008) 1403–1411.
- [39] V. Martínez-Rosas, M.V. Juárez-Cruz, E.J. Ramírez-Nava, B. Hernández-Ochoa, L. Morales-Luna, A. González-Valdez, H. Serrano-Posada, N. Cárdenas-Rodríguez, P. Ortiz-Ramírez, S. Centeno-Leija, R. Arreguin-Espinosa, et al., Effects of single and double mutants in human Glucose-6-phosphate dehydrogenase variants present in the Mexican population: biochemical and structural analysis, *Int. J. Mol. Sci.* 21 (8) (2020) 2732.